Yarn-Level Simulation of Hygroscopicity of Woven Textiles

Aihua Mao, Wenbo Dong, Chaoqiang Xie, Huamin Wang, Yong-Jin Liu, Guiqing Li, Ying He

Abstract—Simulating liquid-textile interaction has received great attention in computer graphics recently. Most existing methods take textiles as particles or parameterized meshes. Although these methods can generate visually pleasing results, they cannot simulate water content at a microscopic level due to the lack of geometrically modeling of textile's anisotropic structure. In this paper, we develop a method for yarn-level simulation of hygroscopicity of textiles and evaluate it using various quantitative metrics. We model textiles in a fiber-yarn-fabric multi-scale manner and consider the dynamic coupled physical mechanisms of liquid spreading, including wetting, wicking, moisture sorption/desorption, and transient moisture-heat transfer in textiles. Our method can accurately simulate liquid spreading on textiles with different fiber materials and geometrical structures with consideration of air temperatures and humidity conditions. It visualizes the hygroscopicity of textiles to demonstrate their moisture management ability. We conduct qualitative and quantitative experiments to validate our method and explore various factors to analyze their influence on liquid spreading and hygroscopicity of textiles.

Index Terms—anisotropic textile, fluid dynamics, physical models, microscopic simulation, liquid-textile interaction

1 Introduction

Hygroscopicity is the measurement of a material's ability to absorb or release water as a function of humidity. Hygroscopicity is a key performance criterion used in moisture management of textiles, such as textiles with low hygroscopicity can quickly transfer liquid from one side to another side, which is called fast-drying ability. Textiles are constructed by porous materials, and their hygroscopicity is determined by a series of complex, microscopic physical processes, including wetting, wicking, moisture sorption/desorption, drip diffusion, and evaporation/condensation [1]. From a microscopic point of view, these mechanisms are influenced by a group of structural factors of textiles, such as surface smoothness, density, thickness, yarn diameter, and porosity.

In computer graphics, simulating textiles and their interaction with other objects has received much attention in the last two decades. Classical approaches model, synthesize, simulate and render fabrics based on yarn-level representations [2], [3], [4], [5], [6]. Recent studies focus on simulating liquid-fabric interaction, such as diffusion [7], stains [8], and bulk liquid [9]. These methods aim to produce realistic visual effects. However, due to the complexity of geometrically modeling the practical anisotropic structure of textile and the limitation of simulated physical mechanisms, the current simulation results still greatly deviate from reality if measured in a quantitative manner. To the best of our knowledge, the quantitative simulation and analysis of liquid spreading and hygroscopicity of textiles are unexplored topics in computer graphics.

In this study, we develop a microscopic method for yarn-level simulation of the hygroscopicity of textiles, which consists of 3D geometric modeling of textiles, fast fluid simulation and physics-driven liquid-textile interaction. Our system can quantitatively simulate liquid spreading on textiles with different types of fiber materials and structures concerning the thermal conditions of the environment. Our simulation produces physics-driven visualization of liquid-textile interaction, which is beneficial for highly realistic animation of micro-scale physical mechanisms and computer-aided design for moisture manageable fabrics.

The main contribution of our work is threefold:

- We propose a microscopic method for yarn-level simulation of the textile's hygroscopic performance, and evaluate it using various quantitative metrics.
- We propose a multi-scale method that constructs textiles in a fiber-yarn-fabric manner to geometrically model the practical anisotropic structure of textiles so that liquid-textile interactions can be simulated.
- We propose a simulator that considers the dynamic coupled physical mechanisms of liquid spreading on textiles, including wetting, wicking, moisture sorption/desorption, and transient moisture-heat transfer, leading to highly realistic simulation results.

- *A.H. Mao, W.B. Dong and G.Q. Li are with School of Computer Science and Engineering, South China University of Technology, Guangzhou, China. E-mails: {ahmao|875158248|ligq}@scut.edu.cn.*
- *C.Q Xie is with School of Software Engineering, South China University of Technology, Guangzhou, China. E-mails: 201921043082@mail.scut.edu.cn.*
- *H.M. Wang (corresponding author) is with Department of Computer Science and Engineering, The Ohio State University, Columbus, OH 43210-1277, USA. E-mail: whmin@cse.ohio-state.edu.*
- *Y.-J. Liu is with BNRist, MOE-Key Laboratory of Pervasive Computing, Department of Computer Science and Technology, Tsinghua University, Beijing, China. E-mail: liuyongjin@tsinghua.edu.cn.*
- *Y. He is with School of Computer Science and Engineering, Nanyang Technological University, Singapore. E-mail: yhe@ntu.edu.sg.*

2 Related Work

2.1 Fluid Simulation

Fluid simulation techniques are roughly classified into Eulerian and Lagrangian methods. The grid-based Eulerian fluid simulation involves the continuous fixed points in space, which supports large-scale flows, such as smoke [10], multiphase flows [11], thin features [12], and accurate contact [13]. The particle-based Lagrangian fluid simulation can model small-scale phenomena with good mass conservation and even simulate the hydrodynamic effects [14].

Many studies have used SPH to simulate weakly compressible fluids [15], [16] and elastoplastic solids [17], to reconstruct the surface of realistic fluid-like splashes and foam [18], and to integrate SPH with Euler grid to improve the simulation effects [19]. Fluid-solid coupling has been widely explored with the SPH framework. The mixture of fluid with solid [20], deformable [21] or porous materials [22] is achieved at the particle-particle level through complex micro-interactions. Futher improvements, such as predictive-corrective incompressible (PCI) SPH [23] and implicit incompressible SPH [24], have been proposed to improve the efficiency and accuracy of pressure force calculation. In this paper, in order to simulate microscopic liquid-textile interactions, we adopt the PCI-SPH model to simulate incompressible liquid wetting across textiles to achieve accurate and efficient fluid modeling.

2.2 Liquid-textile Interaction Simulation

Although cloth simulation has been extensively investigated for more than two decades [25], [26], [27], the interaction between fluids and textiles remains challenging due to complex physical mechanisms. Several approaches have been proposed to simulate fluid flow for porous materials. Lenaerts et al. [22] simulated porous flow in terms of fluid sorption and emission. Patkar et al. [28] reproduced wetting of porous solids including sorption, diffusion, and dripping.

For liquid-texitle interaction, Huber et al. [7] proposed a simulation technique for liquid diffusion on cloth. Chen et al. [29] simulated wet garments for virtual humans. Zheng et al. [8] introduced a technique that can simulate the staining effect on fabrics. Fei et al. [9] proposed a multi-scale model to simulate the bulky interaction between liquid and fabric. However, these studies use either particles or mesh parameterization to represent textiles without considering the practical anisotropic structure and thus cannot simulate the liquid-textile interaction at the micro-scale level. By contrast, our work can simulate the effect of practical geometrical structures on the liquid spreading process and visualize the hygroscopic performance of textiles, which have not been studied before.

For the coupling of liquid and textile, most of the existing researches [7], [9], [28] adopt a two-way coupling framework of particle-based fluid and triangle-based cloth, and some methods [22] use a unified SPH framework. However, the cloth simulation in these studies is simple or just an infinitesimally thin shell, which cannot accurately characterize the complex wetting behavior of textiles. Inspired by these studies, our work builds an interaction framework of SPH liquid and Lagrangian mesh textiles, focusing on geometrical modeling of textiles with practical anisotropic structure to account for the dynamic coupled physical mechanisms at the micro-scale level.

2.3 Physics of Textile Wetting

Theoretically, wetting on textiles is the ability of liquids to maintain contact with the fiber surface and is a prerequisite for wicking, which is driven by capillary force [30]. Wettability is determined by the balance between adhesive and cohesive forces, which are characterized by the contact angle between the fluids on the solid surface.

For porous textiles, liquid spreading and imbibition have been well studied [31]. Washburn [32] established a classical equation describing a liquid flow movement in a perpendicular capillary. Li and Holcombe [33] designed a two-stage moisture sorption model for wool fibers. Lukas et al. [34] used Ising's statistical model to study the wetting behavior of fiber assemblies. Patnaik et al. [35] reviewed the mathematical models of wetting and wicking for fibrous materials.

In the transient phase, heat transfer is coupled with moisture diffusion in four forms, including moisture sorption/desorption and evaporation/condensation. Li et al. [1] investigated the physical mechanisms of moisture diffusion in hygroscopic fabrics, including wetting and wicking through the fibrous space, sorption/desorption by fibers, and liquid diffusion through fabrics, and proposed a coupled fluid and heat transfer model to simulate the interrelated processes [36] [37].

In computer graphics, previous studies on fluid simulation [7], [8], [9], [29] are physically based on the mechanisms of liquid diffusion. However, few of them consider the phase changes due to heat influence, such as moisture absorption/desorption and moisture evaporation/condensation. Our work is the first to assemble dynamically coupled heat and moisture transfer models into the physics-driven simulation and visualization of liquid-textile interaction to achieve highly realistic simulations of liquid spreading on textiles.

2.4 Textile Modeling

Textile modeling and rendering have been studied extensively in computer graphics. Traditional surface models can produce high-quality visual appearance [38] but fail to characterize the structural variation of fabrics. Volume-based approaches address this challenge by modeling varying densities and thicknesses of fabric or fiber silhouettes; e.g., Jakob et al. [39] proposed a physically based volume rendering method for anisotropic scattering structures, and Schroder et al. [39] estimated a parametrized cloth model from a single image. Although these models depict 3D textiles, they still lack yarn-level reality or rely seriously on parametric models. Recently, Zhang et al. [40] reported a tessellation approach for woven fabrics rendering. Cirio et al. [41] introduced a discretization of interlaced yarns for woven cloth simulation at the yarn level. Zhao et al. [42] proposed an automatic fitting approach to create high-quality procedural yarn models with fiber-level details. In our study, inspired by the work [42], we construct a textile model using warp and weft yarns to achieve realistic textile representation with practical anisotropic structures.

3 Overview

We focus on quantitative simulation of micro-scale liquid-textile interaction and visualization of the hygroscopicity of yarn-based textile during liquid spreading. To geometrically model the anisotropic structure, we construct textiles in a fiber-yarn-fabric manner. Most existing approaches usually take particles or parameterized meshes as input textiles, and they do not model the void space between the interlaced yarns and cannot form capillary tubes to initiate liquid diffusion within the textiles. Different from these approaches, we consider the dynamic coupled physical mechanisms that allow us to observe the liquid spreading at a fine scale and to accurately visualize the hygroscopicity of textiles.

Our system consists of three modules: textile reconstruction, fluid simulation, and fluid-textile interaction (shown in Figure 1). To represent liquid at a microscopic level, we use the Lagrange-based SPH method [43] and a PCI-SPH framework [23] to effectively reduce computational cost. In addition to the forces such as pressure and viscosity, we consider that the surface tension and the contact angle between the fluid and the textile surface are nonnegligible factors. The textile is constructed by using an engineering procedure that mainly involves yarn segment twisting from regular and flyway fibers and fabric weaving by interlaced yarn cross units. Hierarchic bounding boxes are built to cover the textile and involve yarn segments and to facilitate the collision detection for liquid-textile coupling. The fluid particles and the 3D structural textiles are coupled through collision detection, which is driven by an assembly of physical models that comprehensively describe the wetting, wicking, moisture sorption/desorption, and coupled moisture-heat transfer occurring in textiles. Our system simulates liquid spreading on textiles using quantitative evaluation metrics and visualizes the water content contained in textiles. Our system can also analyze the influence of fiber materials, textile structure, and environment conditions on the liquid spreading and hygroscopicity of the textile in a visual way.

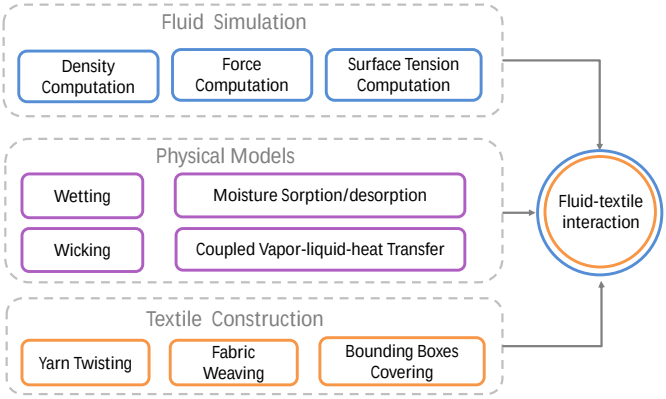

Fig. 1: System overview.

4 Textile Construction

Textiles are porous materials. In spite of their anisotropic nature, textiles are often represented by particles, triangle meshes, or volumetric models with a thickness parameter for simplicity in previous studies [7], [9], [22], [28]. These simplified models are efficient to produce good visual effects. However, they cannot support quantitative simulation due to the lack of microscopic structure modeling of textiles. To address this issue, we model textiles using a multi-scale fiber-yarn-fabric representation that supports physical simulation with yarn-level details.

A textile is a network of yarns. Yarn is produced by spinning raw fibers of wool, flax, cotton, hemp, and other materials to produce long strands. Textiles are formed by weaving, knitting, crocheting, knotting, tatting and felting. We focus on woven textiles due to different methods of making textiles. These textiles are made of warp and weft yarns, which are interwoven at right angles to each other on the plane of the textile. An intersection unit is formed by bending warp and weft yarns under a braiding angle. Woven fabrics often appear coarse due to flyaway fibers deviating from the main stream of yarns. We adopt Zhao et al.'s method [42] to model hair-type and loop-type flyaway fibers. The loop-type flyaway fiber is converted from a regular fiber with a bending radius, and its two endpoints are still inside the yarn body. The density and the bending radius of this fiber offer the visual cue of twisting tightness of the fibers. The hair-type flyaway fiber contributes to the yarn's hairy appearance and is generated by randomly adding short arc fibers with variable lengths and tangent directions, of which only one endpoint is inside the yarn body.

Figure 2 shows the multi-scale pipeline of our textile construction: the fibers are twisted to form yarn segments with the regular part and the flyaway fibers. The warp and weft yarn segments are then interlaced to weave an intersection unit. A woven fabric is finally produced by applying a procedural fiber-yarn-fabric model. Various types of textiles can be simulated through the descriptive parameters of the fabrics that are determined by the yarn and fiber parameters. We use the following four parameters to describe the structure of the fabrics:

Fabric Thickness h_f. Thickness is the main volumetric parameter for a fabric layer. The thickness of a woven fabric is determined by the yarn diameter and the height of maximum loop-style flyaway fiber on the two sides of the fabric:

$$h_f = d_y^p + d_y^t + 2h_a + maxh_l^t + maxh_l^b, \tag{1}$$

where d_y^p and d_y^t are the aggregated diameters of all constituent fibers in the warp and weft yarns respectively, h_a is the arch height of interlaced yarns (shown in Figure 3), $maxh_l^t$ and $maxh_l^b$ are the maximum heights of the flyaway fibers on the top and bottom fabric surfaces, respectively.

Fabric Density ρ_f. Woven fabric density counts the number of yarns per inch and is described as warp and weft densities (ρ_f^p, ρ_f^t) in their directions. It can be interpreted as the number of intersection points between the warp and weft yarns. This parameter can be used to calculate the braiding angle of interlaced yarns and the cross-section area.

Given the unit fabric length in the warp direction (l_f^p), the number of intersection points on a warp yarn is $n_i^p = \rho_f^t$, and the horizontal length of each intersection unit is $l_i^p = 2l_f^p/\rho_f^t$. As shown in Figure 3, we can calculate the braiding angle of the interlaced yarns as

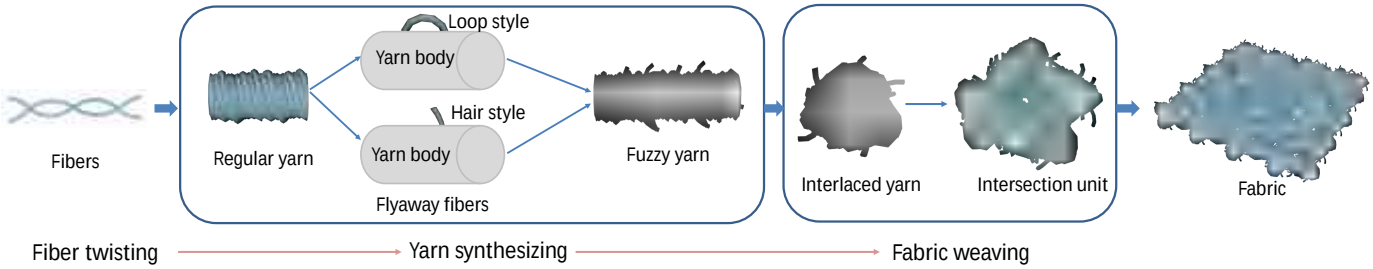

Fig. 2: Multi-scale construction of textiles.

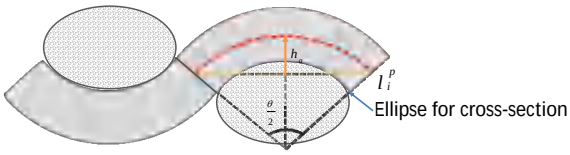

Fig. 3: Interlaced yarns under a braiding angle.

$$\tan\frac{\theta}{2} = \frac{l_i^p}{2(d_y^p + h_a)}, \tag{2}$$

The cross-section area between warp and weft yarns can be approximated as the area of an ellipse between them, i.e., $S_c = 2\pi l_i^p h_a / \sin\frac{\theta}{2}$.

Fabric Surface Smoothness M_f**.** Woven fabrics have different surface smoothness due to different materials and weaving technologies. For example, polyester-made fabrics are smoother than wool-made fabrics. Hair-type flyaway fibers are the main cause of surface roughness. We quantitatively measure the fabric surface smoothness as

$$M_f = 1 - \frac{V_{fly}^l + V_{fly}^h}{V_f}, \tag{3}$$

where V_f is the fabric volume, V_{fly}^l and V_{fly}^h are the volumes of the loop- and the hair-type flyaway fibers respectively, which can be calculated by their densities ρ_{fly}^l and ρ_{fly}^h.

Fabric Porosity ε_f**.** Porosity is defined as the ratio of the free space to the fiber in a given volume of fabric. To simplify the computation, we use the volume ratio of solid fiber materials to the total fabric volume, i.e., $\varepsilon_f = 1 - \rho_{fib}/\rho_f$. From a structural viewpoint, fabric density has a great influence on the capillary performance. The higher the density of fabric, the smaller the capillary radius, and the more difficulty of liquid transmission. The roughness caused by flyaway fibers affects porosity to a certain extent. In this case, we consider the influence of flyaway fibers on the porosity by $\varepsilon_f - k_r(1 - M_f)$, where k_r is the roughness coefficient.

We construct two single-layer woven fabrics by using the fabric parameters of real samples (Figure 4). The similarity between the real and synthetic textiles demonstrates the effectiveness of our textile construction method, which allows us to model the practical anisotropic structure of textiles and simulate the liquid-textile interaction.

Different from previous works [7], [8], [9], [22], [28], [29], our method takes into account the practical anisotropic structure and can accurately simulate the results of fluid flow across 3D porous textiles. Our method follows [42] to represent the yarns as regular and flyaway fibers, and improves [42] by using a multi-scale engineering pipeline in the fiber-yarn-fabric manner to construct the textiles. In our method, there is a strong geometric inference between yarn and fabric structures, which can be used to construct the textiles with various geometrical structures. Thus, the interaction between fluid and textile can be simulated within the textile by using geometrical anisotropic structures based on the yarn-level textile modeling. The textile's hygroscopic performance can be accurately visualized in a measurable manner.

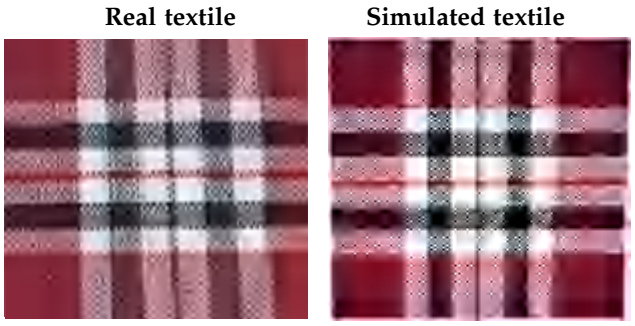

Parameters	Textile 1	Textile 2
Thickness (mm)	0.9	0.8
Surface Smoothness	0.88	0.73
Porosity	0.092	0.103
Warp Density (threads/cm)	34	27
Weft Density (threads/cm)	34	27

Fig. 4: Visual comparison between real and synthetic textiles.

5 Fluid Simulation

To simulate the liquid-textile interaction at the yarn level, we use the SPH model to represent the liquid, which is suitable for the computation on the interface between different materials. Using the particle-based method, we can quantify the volume fraction of liquid sorption/desorption and diffusion during wetting and wicking subject to physical constraints. The attributes A_i (such as density, pressure and viscosity) associated to a particle i can be interpolated by the values of the particles surrounding it [43]:

$$A_i(\vec{r}) = \sum_j m_j \frac{A_j}{\rho_j} W(\overrightarrow{r_{i,j}}, h) \tag{4}$$

where j is a neighboring particle of i, ρ_j is the liquid density of particle j, m_j and A_j are its mass and attributes, $W_{ij}^h = W(\overrightarrow{r_{i,j}}, h)$ is the smooth kernel function with the kernel radius h, and $\overrightarrow{r_{i,j}}$ is the distance between particles i and j.

Solving pressure Poisson equation in the SPH model is computationally expensive. To reduce the computational cost, we adopt the PCI-SPH method [23] that calculates the density and the density variation of a particle in the next time step and updates the pressure from the correction of variation.

In the fine-scale fluid simulation, surface energy plays an important role in determining the shape of fluid when it is interacting with other objects. For liquid-textile interaction, the surface tensions at the solid-vapor, solid-liquid, and liquid-vapor interfaces determine the wettability of a textile. To avoid particle splashing in the traditional method [44], we use a free surface energy function in the diffusion interface model [12] to calculate the surface tension, which is the sum of attraction forces caused by neighboring surface particles, i.e.,

$$F_i^s = \frac{k}{2} \sum_j V_j \left(\frac{|\nabla c_i|^2 + |\nabla c_j|^2}{2} \right) \nabla_i W_{ij}^h, \tag{5}$$

where V_i and V_j are the volumes of particles i and j respectively, and $\frac{k}{2}|\nabla c|^2$ is the density of surface tension energy. The pressure force (F_i^p) and the capillary force (F_i^c) on the particles can be calculated similarly.

6 Liquid-textile Interaction

Given the SPH-based fluid and a 3D textile, we simulate the microscopic liquid-textile interaction by using a particle-solid coupling scheme that detects collision between the particles and the textile. Using the anisotropic structure of textiles, the movement of particles inside the textile is fully driven by hydrodynamics and the physical mechanisms of liquid spreading on the textile. Different from previous studies that ignore the influence of heat flow on moisture transmission, we consider the dynamic coupled physical behaviors, including wetting, wicking, moisture sorption/desorption, and transient moisture-heat transfer across the textile.

6.1 Physical Models

The fibrous textile can be divided into volume fractions of liquid, solid (fibers), and vapor (air) at a discretization element, and their distributions satisfy

$$\varepsilon_l + \varepsilon_a + \varepsilon_f = 1, \tag{6}$$

where ε_l, ε_a, ε_f are the volume ratios of liquid, vapor (air) and fibers respectively.

Transporting liquid through a textile is an anisotropic and nonlinear capillary penetration process. When liquid contacts with a textile, a sequence of liquid-fiber interactions (including wetting, wicking, sorption, and diffusion) occur. We describe each stage as follows:

Wetting. In kinetics, wetting of textile fibers, which is a prerequisite of wicking, is the displacement between a fiber-vapor (air) interface and a fiber-liquid interface [45]. In order for a liquid to moisten a sold, the solid surface should have sufficient energy against the surface free energy of the liquid, which is usually quantified as surface tension. When reaching the equilibrium, the surface tensions at the solid-vapor, solid-liquid, and liquid-vapor interfaces $(\gamma_{sv}, \gamma_{sl}, \gamma_{lv})$ satisfy the Young-Dupre equation:

$$\gamma_{sv} + \gamma_{sl} = \gamma_{lv} \cos\theta, \tag{7}$$

where θ is the contact angle between the tangents to the liquid-vapor (air) interface and the tangents to the solid-liquid interface. Contact angle is often used to measure the wettability of a textile. The smaller the angle, the better the wettability; conversely, the closer the angle to 90°, the worse the wettability. Material is called hydrophilic if it has good wettability, and otherwise called hydrophobic.

Wicking. The wicking of liquid into fabrics can be categorized into four wicking processes [46], namely, immersion, transplanar wicking, longitudinal wicking, and droplet wicking. In this study, we focus on droplet wicking by spreading a liquid droplet into a fabric and quantitatively analyze the hygroscopicity of the fabric.

To take the geometric structure of a textile into consideration, we treat the constituent yarns as capillary tubes. This treatment allows us to model the fiber assembly as a bundle of parallel capillary tubes. Liquid wicks into the capillary tubes following the wetting process on the fibers and is subject to the differential capillary pressure across the liquid-air interface. The liquid is dragged along the capillary by pressure P due to the curvature of meniscus in the narrow confines of the tube, which is calculated by using the equation [31]:

$$\Delta P = P - \rho_l g h, \text{ and } P = \frac{2\gamma_{lv}\cos\theta}{R_c} \tag{8}$$

where R_c is the radius of a capillary tube, ρ_l is liquid density, g is gravitational acceleration, and h is the wicking height.

The mass transfer rate during liquid wicking through the fibrous textile is determined by pressure gradient ∇P across the capillary. The liquid stops rising in capillary penetration when the pressure force is balanced with the gravitational force [32], which can be formulated as:

$$2\gamma_{lv}\cos\theta = R_c \rho_l g h_{eq}, \tag{9}$$

where h_{eq} is the equilibrium wicking height. Gravity acts on the vertical capillary, and will be removed in the horizontal capillary where the wicking height will rise indefinitely.

Moisture sorption/desorption. When a textile is placed in a humid environment, the water content of fibers reaches equilibrium by its moisture sorption/desorption mechanisms; this condition is a nonlinear dynamic process and is influenced by the humidity and the temperature of surrounding micro-environment [31]. The moisture sorption kinetics of fibers is a two-stage process, including a Fickian diffusion and a slower non-Fickian diffusion, which was experimentally discovered by Watt in 1960 [47]. Using Li's model [33], we can model this two-stage of sorption as a uniform Fickian diffusion equation:

$$\frac{\partial C_f(x,r,t)}{\partial t} = \frac{1}{r}\frac{\partial}{\partial r}\left(rD_f\left(w_c,t\right)\frac{\partial C_f(x,r,t)}{\partial r}\right) \tag{10}$$

where C_f is the moisture concentration in the fiber, r is the fiber radius, w_c (%) is the absorbed water content in the fiber, D_f is the diffusion coefficient of the fiber. This model uniformly expresses the two-stage of sorption through D_f, which has different calculation methods in different stages [1]. The benefit of Li's model is that it can model the transient nonlinear sorption while most of previous works ignored or simplified this process by parameters. Moreover, the predictions from this model shows good agreement with experimental observations obtained from the sorption-cell experiment (see page 90 in [48]).

Coupled moisture-heat transfer. Although the interactions between heat and moisture flows are not considered in steady-state conditions, under the transient situations these two processes are coupled and interact mutually and significantly through the phase change processes [49], such as moisture sorption/desorption and evaporation/condensation. During moisture sorption by fibers, heat is generated and released. Consequently, the temperature of fibers increases, resulting in an increase in heat flow across the textile. When the fibers are saturated, moisture desorption may occur on the fiber surface and heat is consumed, thereby leading to a decrease in fiber's temperature. Similarly, liquid condensation/evaporation into or from water vapor is another important phase change process, which affects the heat and moisture flows of the textiles. Thus, the simulation of moisture diffusion across textiles should include the heat transfer to achieve accurate results when phase change processes occur under transient situations. We consider the interactive moisture and heat transfer, and integrate the moisture sorption/desorption, condensation/evaporation and diffusion into the dynamic coupled physical models to drive the simulation.

The influence of heat was not discussed in the graphics literature [7], [8], [9], [22], [28], [29], since they aim at visually pleasing results of liquid-textile interaction and the simulation accuracy is not a major concern. Actually, in practice heat is always an important factor to impact on the liquid diffusion, such as the skin temperature of human body for clothing, the air temperature of environment for wall clothes, carpets and cushions. We will discuss the influence of heat factor in the ablation study in Section 7.2.

The first coupled heat and moisture transfer model was developed by Farnworth in 1986 [50] and improved by Li and Zhu [7] through incorporating the two-stage moisture sorption model [36]. Mao and Li [37] later extended this model with measurable indices to describe the multi-dimensional liquid moisture diffusion in textiles, which provides a potential way for the model to be parameterized with measurable data and effectively applied in engineering applications. On the basis of the mathematical models reported in [37], we numerically represent the transient moisture and heat transfer across the textile in a small unit through three balance equations (see Eqs.(11)-(13)), which are coupled through phase change processes. Eqs. (11) and (12) are the water vapor and liquid balance equations that describe the accumulated water vapor and liquid in the textile during water vapor diffusion $t1$ and liquid diffusion $t3$. Eq. (13) is the heat balance equation that describes the accumulated heat in the textile through heat conduction $t5$. The accompanying phase change processes couple the three balance equations, including water vapor sorption/desorption by fibers $t2$ and liquid sorption/desorption by fibers $t4$, moisture condensation/evaporation Γ_{lg}, and heat release/consumption by moisture sorption/desorption $t6$ and condensation/evaporation $\lambda_{lg}\Gamma_{lg}$:

$$\varepsilon_a\frac{\partial C_a}{\partial t} = \underbrace{\frac{D_a\varepsilon_a}{\tau_a}\frac{\partial^2 C_a}{\partial x^2}}_{t1} + \underbrace{\omega_a\varepsilon_f\Gamma_f}_{t2} - \Gamma_{lg} \tag{11}$$

$$\frac{\partial(\rho_l\varepsilon_l)}{\partial t} = \underbrace{\frac{1}{\tau_l}\frac{\partial}{\partial x}\left(D_l\frac{\partial\left(\rho_l\varepsilon_l\right)}{\partial x}\right)}_{t3} + \underbrace{\omega_l\varepsilon_f\Gamma_f}_{t4} + \Gamma_{lg} \tag{12}$$

$$c_v\frac{\partial T}{\partial t} = \underbrace{\frac{\partial}{\partial x}\left(K(x,t)\frac{\partial T}{\partial x}\right)}_{t5} + \underbrace{\kappa\varepsilon_f\Gamma_f}_{t6} - \lambda_{lg}\Gamma_{lg} \tag{13}$$

where C_a is water vapor concentration filling in the inter-fiber void space, D_a is the water vapor diffusion coefficient through the textile, D_l is the liquid water diffusion coefficient through the textile, which is determined by the capillary and gravity effect, and can be calculated as [36]:

$$D_l = \frac{3\gamma_{sl}\cos\theta\sin^2\beta R_c\varepsilon_l}{20\eta\varepsilon}, \tag{14}$$

η is dynamic viscosity and β is the intersection angle between the barycenter of the yarn segment and the gravity. τ_a and τ_l are water vapor and liquid water diffusion tortuousity, ω_a is the proportion of the sorption of water vapor and equal to $\frac{\varepsilon_a}{1-\varepsilon_f}$, ω_l is the proportion of the sorption of liquid and equal to $\frac{\varepsilon_l}{1-\varepsilon_f}$. $K(x,t)$ is the thermal conductivity of porous textile, $\kappa = \omega_a\lambda_v + \omega_l\lambda_l$, and λ_v, λ_l are the latent heat of sorption of vapor or liquid. Γ_f is the moisture sorption/desorption rate of fibers in Eq. (10) and N is the number of fibers constitution in the yarn. Γ_{lg} is the moisture evaporation/condensation rate at the local temperature T :

$$\Gamma_{\mathrm{lg}} = h_{\mathrm{lg}}S_v\left(C^*(T) - C_a\right), \tag{15}$$

S_v is the surface/volume ratio of the fiber, h_{lg} is the mass transfer coefficient for evaporation and condensation.

We refer the readers to [37] for the details of the boundary conditions of Eqs.(11)-(13) and the finite-volume solution for them. This transient moisture-heat model is more

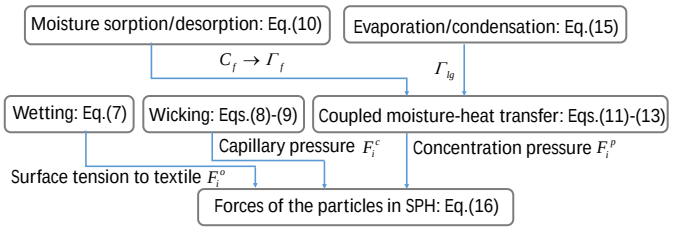

Fig. 5: Incorporation between different physical models for liquid-textile interaction.

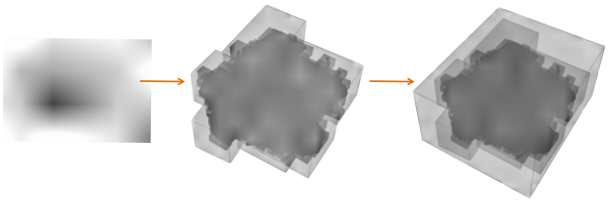

Fig. 6: Hierarchical bounding boxes of yarn segments, cross units and textile.

accurate than the liquid diffusion model in simulating the liquid spreading on textiles with influence of temperature.

Figure 5 shows the incorporation between the physical models reported above. These models respectively contribute to the calculation of surface tension, capillary and concentration pressure force for the SPH-based fluid simulation (see Eq. (16)). The equation solver for all the physical models and the default values or calculation methods of all involved parameters in the models are listed in the appendix.

6.2 Physics-driven Coupling

The particle-based liquid is coupled with the 3D textile model when the liquid comes to contact with the textile. The microscopic interaction between the liquid and the textile driven by the above physical mechanisms is achieved by collision detection between the particles and the textile surface. The textile is constructed by anisotropically structured yarn segments that are modeled by triangle meshes. The exhaustive method to detect each particle and each mesh leads to extremely expensive computation. Thus, we construct hierarchical bounding boxes to cover the yarn segments, intersection units, and textile, as shown in Figure 6, An AABB bounding box tree is created to fit with the yarn segments and used to replace the numerous triangle meshes of fiber surface for collision detection. The particles are detected with the AABB bounding box tree of a yarn segment only when they enter the bounding box of the textile and the bounding box of a cross unit. The hierarchical bounding boxes greatly reduce the computational complexity of collision detection through level-by-level filtering.

During collision detection, the contacted particles are absorbed into the bounding box and removed from the SPH if the water content of a yarn segment w_{ys} is under saturation. Otherwise, the contacted particles are bounced with a loss of momentum $q_{loss} = k_l m v_0$, where k_l, m, v_0 are the loss coefficient, mass, and velocity of the particles, respectively. An approaching particle v_0 moves along the yarn surface with a frictional force when its velocity is below a threshold (T_v). This particle is evaluated by μmg and μ is the frictional coefficient of textile material. Occasionally, the particle has extremely fast velocity to penetrate through the bounding box within a frame time. We predict the position of the particle for the next frame after detection in the current frame and apply a repulsive force related to the particle's velocity to prevent its penetration .

The mass of absorbed particles into a yarn segment (m_p^i) is aggregated and mapped to the water content of yarn segment (w_{ys}^i). As described in Eqs. (10)-(13), the water content of the fiber is dynamic due to the influence of the humidity and the temperature of the surrounding micro-environment. The water contents of every yarn segment, which are aggregated by all composed fibers, can be computed at each time step. Once m_p^i reaches the saturated water content, the particles absorbed in the yarn segment possibly diffuse to the connected yarn segments on the two sides and the interlaced yarn segment in accordance with the difference in water contents between them $\Delta w_{ys}^{i,j}$, which forms a gradient vector. We only allocate the mass of absorbed particles from m_p^i to m_p^j to represent the diffused particles because the particles diffusing inside the yarn segment are invisible.

In theory, diffusion inside a yarn segment toward connected yarn segment is greater than that toward interlaced yarn segment. Thus, the allocated mass of particles to the interlaced yarn segment is alleviated by an obstruction coefficient η. The liquid inside a yarn segment is desorbed outside when the level of saturated water content of a yarn segment is decreased and no water content gradient is found to its connected and interlaced yarn segments. In this case, new particles are randomly generated on the bounding box surface of the yarn segment rather than on the meshed surface of fibers to achieve a better efficiency. The mass of new particles m_p^d is dependent on the decreased water content for saturation, namely, $m_p^d = k_{mapping}(w_{ys}^s - w_{ys}^{s'})$.

For particles that are not absorbed into the yarn segment during collision detection, they continuously move in the pores of textile driven by capillary. Except the original forces described in the SPH model, which mainly include the forces by the pressure on particles and the viscosity [51], the particles will be additionally exerted the capillary force and gravitational force and even the frictional force. Thus we compute the forces for the particles as:

$$F_i(t) = F_i^p + F_i^v + F_i^c + F_i^g + F_i^o, \tag{16}$$

where $F_i^p, F_i^v, F_i^c, F_i^g$ mean the forces caused by the pressure gradient, viscosity, capillary and gravity. F_i^o can be the surface tension force or possible frictional force for the particles on the interface of fiber and liquid, and the frictional force is determined by the surface smoothness of yarns. The deduction and calculation methods for F_i^o, F_i^p, F_i^v, F_i^c can be found in the appendix. Figure 5 shows the contributions of the physical models to these forces. When all the forces acting on the particles are exactly balanced, the diffusion stops. Otherwise, the particles can penetrate the pores to the other side and cause dripping.

7 Implementation and Evaluation

The simulation is implemented in three modules, including textile construction, liquid simulation by PCI-SPH, and

liquid-textile interaction. First, the textile is constructed in accordance with the fiber material and structure parameters. Given different configurations, the virtual textile can be modeled with various patterns of the real textile. Second, the fluids of liquid droplets are simulated with the PCI-SPH method. Third, during liquid-textile interaction, the particles are basically exerted by the forces of pressure, viscosity, and gravity, and are updated by adding capillary pressure when they flow through the capillary pores of the textile, which is indicated by the condition that the particles have already come into the bounding box of textile but have no contact with the bounding boxes of yarns.

To accelerate the computation, we predict the viscosity and density in advance and then compute their pressure. With the solution from the physical models, the simulation of liquid-textile interaction can be achieved in a physically driven manner. Finally, the yarn segment is mapped with different colors and brightness to indicate the different volumes of water contents.

All simulation experiments were conducted on a PC with a 3.5 GHz CPU and a Nvidia GTX1650 GPU with 4GB GPU memory. Each yarn is twisted by 30 constituent fibers. Table 1 reports the computation time for each simulation step and one droplet spreading. Each liquid droplet is composed by 8,000 particles in the simulation. We observe that collision detection between particles and bounding boxes is the most expensive one.

TABLE 1: Computational cost of simulation.

Components	Average time (s/simulation)	# Particles
Constructing textile ($/cm^2$)	47	-
Solving physical models	140	-
Collision detection($/$iteration)	4.8	-
Simulating one droplet spreading	900	8000

To evaluate the accuracy, we compare the simulated and actual results. Comparing the simulated and actual results at a certain moment is insufficient because the liquid spreading across the textile is a nonlinear dynamic process with time. Thus, we make a qualitative comparison with the real experiment in the whole spreading process of a liquid droplet and a quantitative comparison with the experimental measurement on the final liquid spreading results based on the maximum wetting radius (MWR). The fiber material and structure properties of the textiles (A, B, C, and D) used in all simulation cases are listed in Table 2.

7.1 Droplet Spreading Experiment

Two cotton textiles (A and B) made with different structure properties were used to perform the experiment. A droplet of liquid water was dripped on the textile, and an optical microscope was used to record the whole liquid spreading process across the textiles. We simulated these liquid spreading processes on the constructed cotton textiles in accordance with the constituent material and structure of the real textiles. Figure 7 shows the comparison of the simulated and real experimental results on five moments in the whole continuous spreading process. These experiments demonstrate that our simulation is similar to real-world results.

7.2 MWR Measurement

MWR is an important index of spreading rate in the American Association of Textile Chemists and Colorists (AATCC) standard test method 195-2011 [52], which is developed to characterize the dynamic liquid moisture transfer in porous textiles. When testing with a specific instrument (named MMT [53]), a predefined amount of liquid is introduced to the fabric sample with size of 8cm$\times$8cm, and MWR measures the maximum radius of the wetting area on the top and bottom surfaces when the liquid spreading is completed. By referring to the measurement experiment of liquid moisture management properties on hemp woven fabrics using MMT in [54], we construct the same fabrics (textiles C and D), and simulate the liquid spreading process with the same testing condition of air temperature 20°C and relative humidity 65% in [54]. To calculate the MWR on the rendered simulation results, we treat it as a minimum enclosing disk problem and use the algorithm reported in [55] to realize automatic measurement. The comparison between the simulated and real measured MWR of textiles C and D is shown in Figure 8. The red rings generated by the algorithm fit well with the maximum wetting areas, and the radii of the rings are the predicted MWR. The error rates between the real measured MWR and the predicted MWR are 5.6% and 4.8% for textiles C and D, respectively. This finding indicates that the simulation results are in good quantitative agreement with the actual experiment.

Meanwhile, we also conduct an ablation study of different simulation models in terms of the error rate in the MWR measurement. As shown in Table 3, when the heat model (Eq.13) or even the coupled heat-moisture transfer model (Eqs.(11)-(13)) is missed in the simulation, the error rate in the MWR measurement increases greatly.

7.3 Comparison with Relevant Works

Due to different goals between our method and the existing approaches, it is difficult to make a direct comparison. Thus, we conduct a qualitative comparison here.

First, previous studies [7], [8], [9], [22], [28], [29] focus on producing visually pleasing appearances of fluid-porous solid interaction. Although their simulation results look realistic, they are still obviously different from real results, and none of these studies quantitatively compare the actual interaction in practice. Thus, it is difficult to evaluate the accuracy of these studies. As a comparison, our simulation results are compared with real experimental results qualitatively and quantitatively. We validate the accuracy of the simulation results using the MWR index in accordance with the AATCC standard test method. Therefore, our method not only provides a realistic appearance, but also enables accurate analysis of the hygroscopic performance of the textile.

Second, to the best of our knowledge, our work is the first to perform the fluid-porous solid interaction simulation based on the practical anisotropic structure of 3D textiles. Previous studies simplify the modeling of porous materials using particles or mesh parameterization. Lenaerts et al. [22] represented porous materials as particles. Patkar et al. [28] and Huber et al. [7] used a mesh-based model for the textile that is only an infinitesimally thin shell. Fei et al. [11]

TABLE 2: Textiles used in simulation.

Name	Fiber material	Yarn diameter (mm)	Textile thickness (mm)	Warp density (threads/cm)	Weft density (threads/cm)
Textile A	Cotton	0.54	1.96	17	15
Textile B	Cotton	1.23	2.83	7	6
Textile C	Hemp	0.4	0.52	25	20
Textile D	Hemp	0.4	0.43	33	28
Textile E	Wool	0.2	1.46	37	37
Textile F	Cotton	0.2	0.635	35	35
Textile G	Polyester	0.2	0.46	28	28

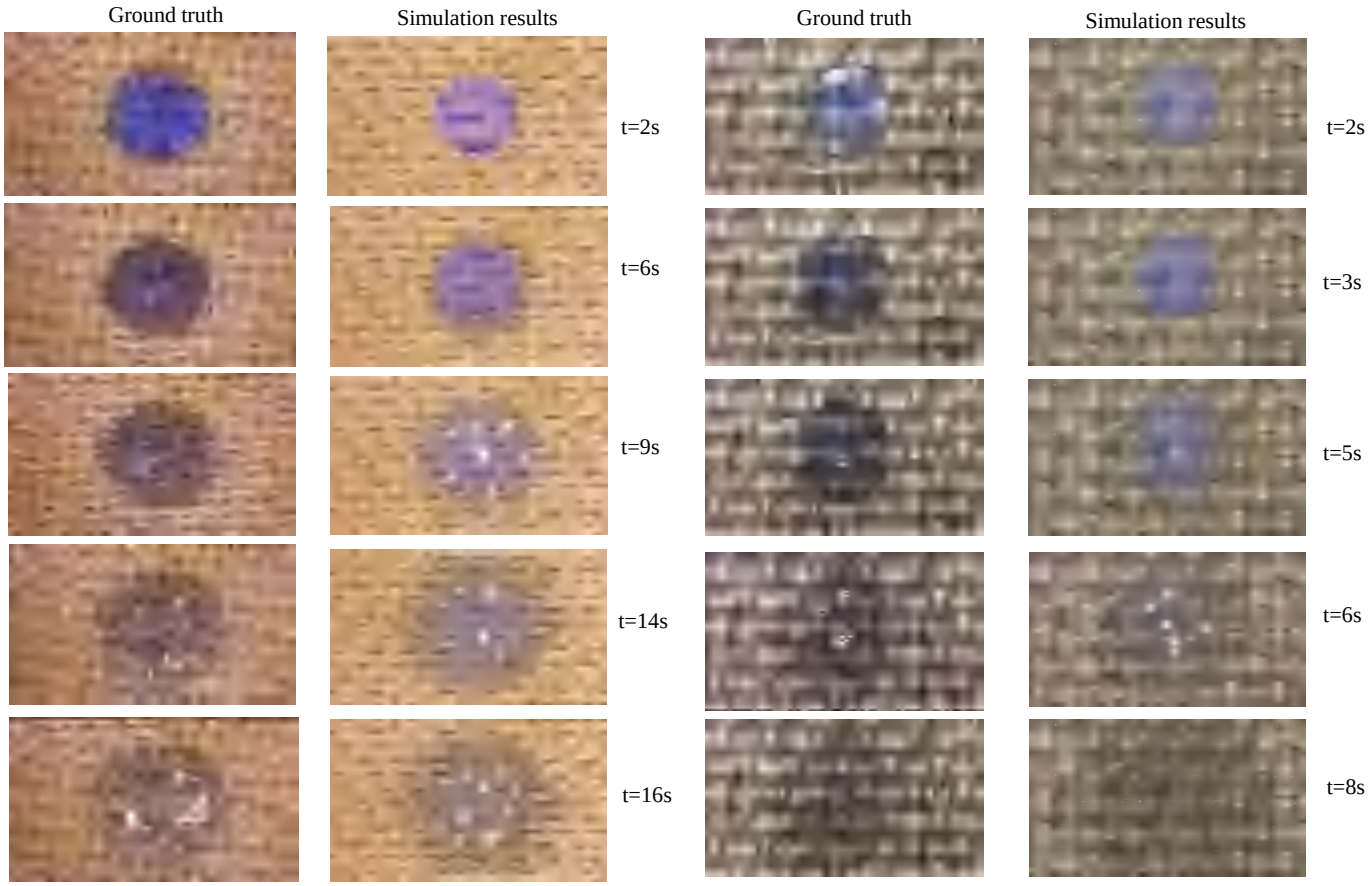

(a) Textile A (b) Textile B

Fig. 7: Comparison between the simulated and the real droplet spreading on textiles A and B.

TABLE 3: Ablation study of different simulation models in terms of the error rate in the MWR measurement.

Measurement textile	Our method	No C1 [1]	No C2 [2]
Textile C	5.6%	19.8%	45.2%
Textile D	4.8%	18.7%	43.6%

[1] C1-heat model
[2] C2-coupled heat-moisture transfer model

modeled the wet fabric as a continuum mixture of water, air, and fabric material. Zheng et al. [8] proposed a triple-layer model to handle the liquid yarn interaction without textile geometric model. These studies cannot geometrically model the practical anisotropic structure of textile to provide a solid foundation for achieving physically accurate simulation. Our work constructs the textile by using a fiber-yarn-fabric engineering pipeline and models realistic textiles with practical anisotropic structures. Thus, our framework can robustly analyze the effects of various materials and geometrical structures on the liquid spreading process and hygroscopic performance of textiles that have not been explored in previous studies.

Third, we consider the dynamic coupled physical mechanisms of liquid spreading on textiles, including moisture wetting, wicking, diffusion, and phase change processes, such as moisture absorption/desorption and condensation/evaporation. These mechanisms are coupled with the effect of heat flow on liquid transmission through the geometry-aware modeling of textiles with capillary pore distribution. All these mechanisms are described by an integrated assembly of physical models. Thus by simulating the interactive moisture-heat transfer on the liquid spreading, accurate simulation results can be obtained. Note that only part of physical mechanisms were considered in previous

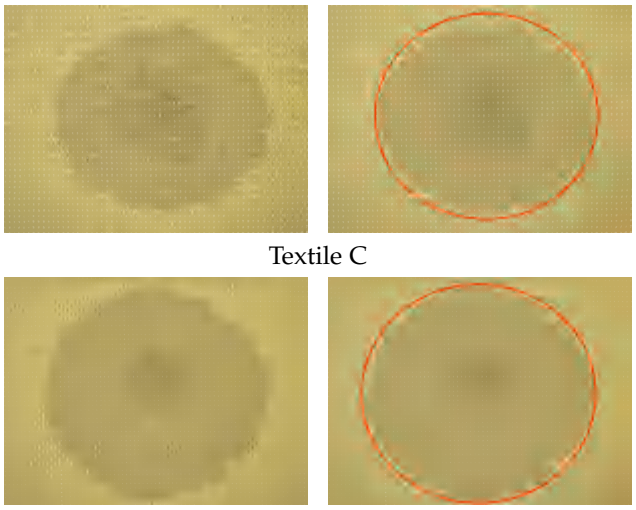

Textile C

Textile D

Fig. 8: Maximum wetting radius of the simulation results of the textiles C and D. The left ones are the simulation result, and the red ring on the right ones fits the maximum wetting area.

studies. Patkar et al. [28] did not explicitly consider the effect of pore size and the simulation of anisotropic diffusion was handled by using image masks. Huber et al. [7] only simulated liquid diffusion in cloth without considering other phenomena, such as wetting and wicking, moisture sorption and evaporation/condensation. Zheng et al. [8] simplified the liquid diffusion using the triple-layer model for visual effect. Fei et al. [9] modeled the macro-scale simulation by calculating the pressure gradient and drag forces. Thus, these studies cannot accurately handle the nonlinear and heat-coupled liquid spreading on textiles. Our work fills this gap and simulates the liquid-textile interaction by taking into account the effect of thermal conditions (temperature, relative humidity) on the liquid spreading, which is consistent with practice.

Table 4 qualitatively compares our work with relevant works, and summarizes the differences from diverse perspectives. Note that our work is built on a quite different pipeline, with major differences in textile modelling, physical models and simulation scale.

Unlike previous works, our method constructs textile in a 3D fiber-yarn-fabric production procedure, resulting in a textile model with practical capillary pores, which enables diffusion simulation driven by more comprehensive physical mechanism, such as non-linear coupled heat and moisture transfer. Our method aims at micro-scale physics-driven simulation, and can achieve results that is both visually and quantitatively consistent with reality. Zheng et al.'s work [8] also focuses on micro-scale simulation, while it uses abstract fabric layer and renders the stains by composition of different masks effects. The micro-scale simulation methods, such as our work and Zheng et al.'s work [8], are more likely to use static or plain textile to better show the microscopic liquid spreading process. Fei et al.'s [9] and Patkar et al.'s [28] methods, which focus on large-scale animation and model the textile by particles or infinite thin shell (i.e., 2D triangle meshes), are more efficient to simulate deformed or wrung textile and obtain macroscopic visual effects.

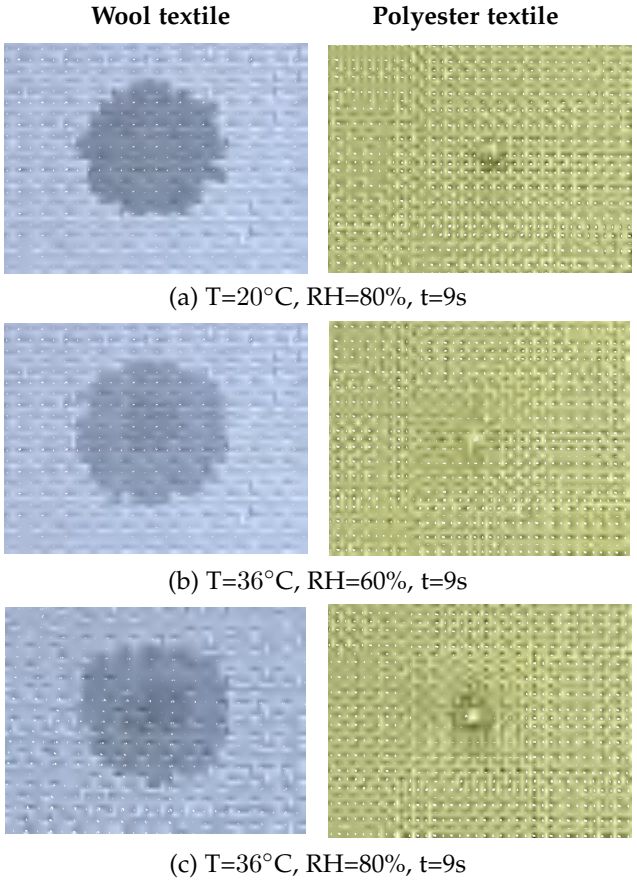

(a) T=20°C, RH=80%, t=9s

(b) T=36°C, RH=60%, t=9s

(c) T=36°C, RH=80%, t=9s

Fig. 9: Liquid spreading on a wool textile and a polyester textile under different thermal conditions.

8 Simulation Experiments

In this section, we demonstrate a series of simulation experiments, including the influence of thermal conditions, different fiber materials, and different fabric geometrical structures on the liquid spreading across the textiles, to show the simulation capability of our method and visualize the hygroscopic performance of textiles. The default thermal conditions in all simulation experiments (except in Section 8.1) are air temperature 25° and relative humidity 65%.

8.1 Environment with Different Thermal Conditions

In physical mechanism, the water absorbability of a fiber is influenced by the temperature and relative humidity of the micro-environment. The physical models used in our method consider the coupled mechanisms of moisture-heat transfer across the textile. Our method can simulate and show the influence of temperature and relative humidity of the environment on the liquid spreading across the textile. Here, we construct two textiles with wool and polyester (textiles E and G) and simulate a water droplet spreading on the textiles in the environments with evolving thermal conditions, namely, air temperature 20° and relative humidity 80%, air temperature 36° and relative humidity 60%, and air temperature 36° and relative humidity 80%. As shown

TABLE 4: Comparison with relevant studies of liquid-textile interaction.

Dimensions	Fei et al. [9]	Zheng et al. [8]	Patkar et al. [28]	Our method
Fluid model	APIC	None	SPH	PCI-SPH
Textile model	Lagrangian mesh	Abstract triple-layer-model	Triangle mesh	3D fiber-yarn-fabric model
Textile structure parameters	2	2	None	9
Capillary pore	Implicit	Implicit	No	Explicit
Textile deformation	Applicable	No	Applicable	No
Liquid diffusion model	Mixture theory	Capillary pressure	Linear Darcy's law	Non-linear Fick's second law
Moisture absorption/desorption	Parameterizations	No	Parameterizations	Non-linear model
Influence of heat	No	Evaporation	No	Coupled moisture-heat
Simulation VS reality	Visually weak match	Visually comparable	Visually comparable	Visually and quantitatively match
Simulation scale	Macroscale	Microscale	Macroscale	Microscale

in Figure 9, the simulated results demonstrate that lower temperature and higher relative humidity help the fabric to absorb more liquid, while higher temperature leads to a fast liquid spreading but less liquid content due to evaporation.

8.2 Textiles with Different Fiber Materials

The moisture absorbability of textile is substantially determined by the moisture regain property of the fiber material. Different fibers have different amounts of moisture regain. For example, wool fiber has high moisture regain, whereas polyester fiber has low moisture regain. Thus, wool textile absorbs more liquid than polyester textile. To compare the hygroscopicity of textiles made by different fiber materials, we choose wool, cotton, and polyester fibers to construct three textiles (E, F, G) with same structural parameters of yarn diameter, twisting, cross-section area and fabric density. We then simulate dripping of three water droplets with a time interval of $3s$ on the chosen textiles. Figure 10 shows the simulated liquid spreading for the first, second, and third droplets. The moisture regain of the wool, cotton, and polyester fibers decreases by 16%, 8.5%, 0.4%, respectively. The wool textile has the best moisture absorbability, thereby the largest wetting radius. The polyester textile absorbs little moisture and spreads with the smallest wetting radius.

8.3 Textiles with Different Geometrical Structures

Contact angles. The contact angle of the textile (θ) significantly influences the surface wettability, that is, the smaller the contact angle, the better the wettability; whereas, the larger the contact angle, the worse the wettability. The textile is regarded as hydrophilic or hydrophobic when the contact angle is close to 0° or 90°. To demonstrate the influence of contact angle, we simulate the dripping of liquid droplets on a cotton textile (the same as textile E) with contact angles of 1°, 60°, and 89°. Figure 11 shows the simulated liquid spreading in these three cases. The textile with contact angle 1° completely absorbs and diffuses the liquid droplets. The textile with contact angle 60° partially absorbs the liquid droplets and leaves some small droplets on the textile surface. The textile with contact angle 89° cannot absorb the liquid droplets, which remain on the textile surface with original shape.

Porosities. The porosity of textile ($\varepsilon_{textile}$) reflects the volume of void space within the total volume of textile and is a crucial property indicating the capillary pore size of the textile. The textiles with different porosities have different performance of capillary diffusion, which is described as the one-way liquid transport capacity from the top surface to the bottom surface of the fabric [53]. We simulate the dripping of liquid droplets on a cotton textile (the same as textile E) with porosities 0.255, 0.184, and 0.102, and demonstrate the wetting area of the top and bottom surfaces in these three cases. As shown in Figure 12, the textile with higher porosity has larger MWR, and more moisture is transported from the top to the bottom. The textile with lower porosity has smaller MWR, and fewer moisture is transported from the top to the bottom due to weak capillary diffusion.

Dimensional simulation. The structure of textile is characterized by a set of parameters, and liquid spreading is influenced by the structure parameters in addition to the contact angle and the porosity. We conduct a multivariable simulation of the liquid spreading on the textile in different dimensions. The variables used are the yarn diameter d_y, warp density ρ_{warp}, weft density ρ_{weft}, and flyaway density ρ_{loop} and ρ_{hair}. We construct a cotton textile with varied values of structure parameters and drip three droplets of liquid successively on different areas of the textile. We change the value of a single parameter while fixing the others to demonstrate the one-way analysis of structure-ware spreading performance.

Figure 13 shows the simulation results of nine cases in three groups. In the first group, the changing variable is the yarn diameter (d_y) of the textile. With the fixed warp and weft densities, the larger value of d_y leads to the smaller porosity of the textile. This parameter reduces the intensity of liquid diffusion through capillary wicking and leads to smaller MWR. In the second group, the changing variables are fabric densities ρ_{warp} and ρ_{weft}. The denser the threads, the smaller the pore sizes between the void space and porosity of fabric, and also the smaller the MWR. In the third group, the changing variables are flyaway densities ρ_{loop} and ρ_{hair} that affect the fabric porosity. The higher the flyaway density, the smaller the fabric porosity in theory. Thus, the liquid spreading has a similar trend in another two groups.

8.4 Potential Applications

Our method provides a microscopic yarn-level simulation of the hygroscopicity of textiles by modelling textiles with practical anisotropic structure and considering coupled non-linear physical mechanisms. As shown in the experimental results above, our method achieves accurate simulation of liquid spreading across textiles with different fiber materials and fabric structures, and under different thermal condi-

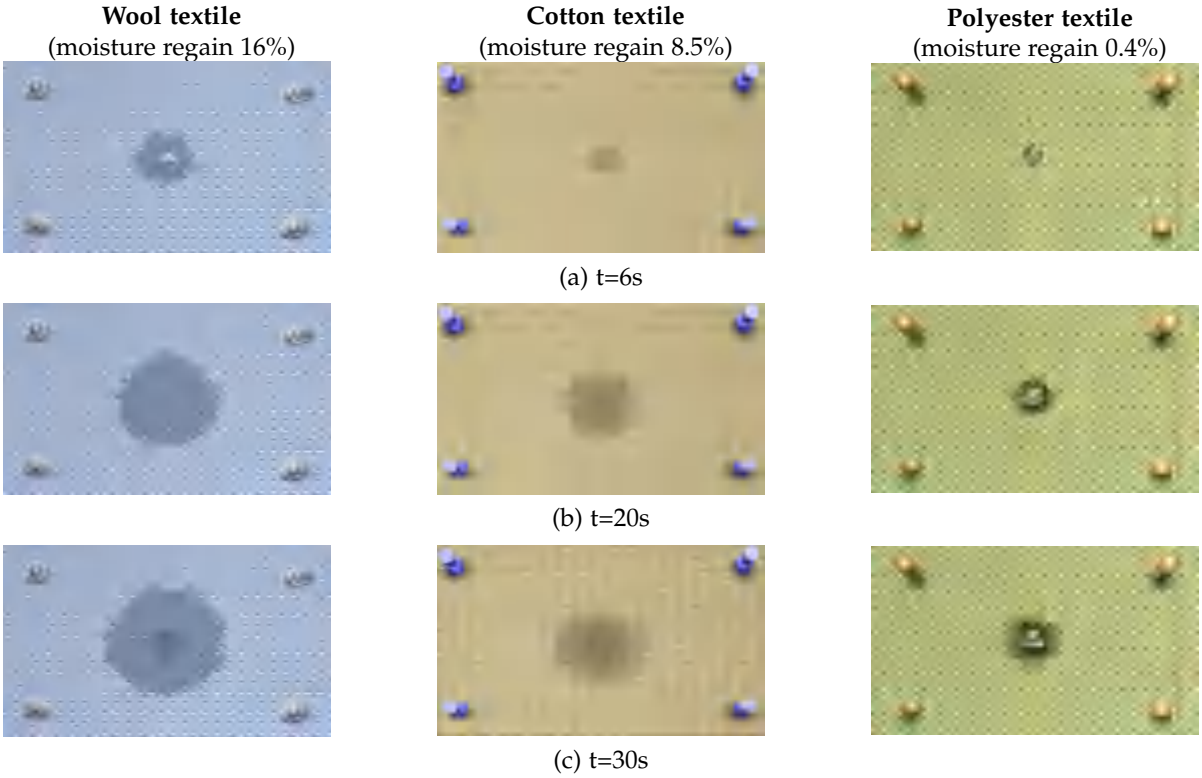

Fig. 10: Liquid spreading on wool, cotton and polyester textiles by three droplets.

Fig. 11: Liquid spreading with different contact angles.

tions. The simulation results agree with the real results both visually and quantitatively. Thus our method has potential for physics-driven graphics applications, such as VR education and accurate physical visualization animation. Figure 14(a) shows an application scenario of 3D VR: a user, wearing VR headset, plays a wetting game by putting water droplets on a textile with a hand controller (in cloth scene 1). The user compares different textile's hygroscopicity performance (in cloth scene 2) and study the properties of textile influencing wetting (in cloth scene 3). Figure 14(b) shows two examples of physical visualization animation including liquid spreading on a pillow and liquid spraying on a flag. See the supplementary video for the animation.

Furthermore, due to the accurate simulation capability, our method can also be used for computer-aided design of textile. Figure 15 shows an application example of a sportswear design, in which we simulate the fabric with some water droplets spreading instead of testing the real samples with an instrument, and preview its hygroscopic performance in a scientific manner. In order to directly observe the textile's hygroscopicity in detail, we divide the textile into grids with four yarn intersection units and aggregate the water content in the unit. Then the designer can determine an appropriate fabric for the sportswear by previewing its hygroscopicity.

9 Discussions and Conclusion

We presented a microscopic method to simulate the hygroscopic performance of textiles at a yarn level. The liquid-textile interaction is based on a practical anisotropic structure of the 3D geometrical textile model by using a multi-scale textile construction pipeline. We take the dynamically coupled physical mechanisms of liquid transmission across the textile into consideration to drive the fluid-textile coupling. Accordingly, our simulation enables accurate visualization of the hygroscopic performance of textiles with different materials, structures and environment. These advances make our method useful in both micro-scale physics-driven graphic applications and computer-aided design of textiles.

Our method has several limitations: (1) It focuses on microscopic simulation, which constructs textile by numerous

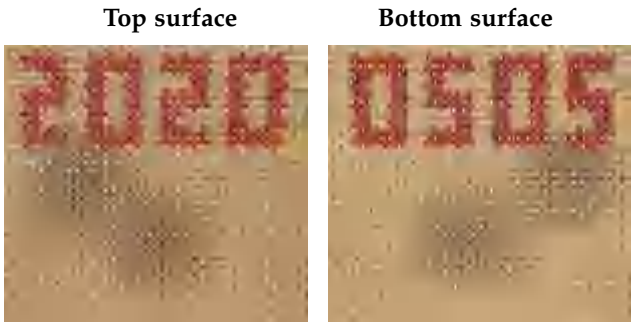

(a) $\varepsilon_{textile} = 0.255$, t=15s

(b) $\varepsilon_{textile} = 0.184$, t=15s

(c) $\varepsilon_{textile} = 0.102$, t=15s

Fig. 12: Liquid spreading on a cotton textile with different porosities. We show the results on both the top and bottom sides.

twisted 3D fibers and interlaced yarns instead of particles or 2D meshes, thus is not efficient on deformed textiles, such as wringing fabrics or swelling fabrics due to saturated water; (2) We only consider pure liquid in our simulation and cannot simulate liquid with substances, such as stain in [8]; (3) Our method has high memory usage for large-sized textiles due to the high-resolution fiber-yarn-fabric model. There are two interesting future directions: (1) designing an efficient representation of the geometrical model of textiles to reduce memory and to efficiently model large textiles, and (2) parallelizing the physical simulation and liquid-solid coupling to achieve high efficiency.

ACKNOWLEDGMENT

We thank the anonymous reviewers for their constructive comments that help us to improve the paper.

REFERENCES

[1] Y. Li and Z. X. Luo, "Physical mechanisms of moisture diffusion into hygroscopic fabrics during humidity transients," *The Journal of The Textile Institute*, vol. 91, no. 2, pp. 302–316, 2000.

[2] J. M. Kaldor, D. L. James, and S. Marschner, "Simulating knitted cloth at the yarn level," *ACM Trans. Graph.*, vol. 27, no. 3, pp. 65:1–65:9, Aug. 2008.

[3] S. Zhao, W. Jakob, S. Marschner, and K. Bala, "Structure-aware synthesis for predictive woven fabric appearance," *ACM Trans. Graph.*, vol. 31, no. 4, pp. 75:1–75:10, Jul. 2012.

[4] G. Cirio, J. Lopez-Moreno, D. Miraut, and M. A. Otaduy, "Yarn-level simulation of woven cloth," *ACM Trans. Graph.*, vol. 33, no. 6, pp. 207:1–207:11, Nov. 2014.

[5] P. Khungurn, D. Schroeder, S. Zhao, K. Bala, and S. Marschner, "Matching real fabrics with micro-appearance models," *ACM Trans. Graph.*, vol. 35, no. 1, pp. 1:1–1:26, Dec. 2015.

[6] V. Narayanan, K. Wu, C. Yuksel, and J. McCann, "Visual knitting machine programming," *ACM Trans. Graph.*, vol. 38, no. 4, pp. 63:1–63:13, Jul. 2019.

[7] M. Huber, S. Pabst, and W. Straßer, "Wet cloth simulation," in *ACM SIGGRAPH 2011 Posters*. ACM, 2011, p. 10.

[8] Y. Zheng, Y. Chen, G. Fei, J. Dorsey, and E. Wu, "Simulation of textile stains," *IEEE Transactions on Visualization and Computer Graphics*, vol. 25, no. 7, pp. 2471–2481, 2019.

[9] Y. R. Fei, C. Batty, E. Grinspun, and C. Zheng, "A multi-scale model for simulating liquid-fabric interactions," *ACM Trans. Graph.*, vol. 37, no. 4, pp. 51:1–51:16, Jul. 2018.

[10] T. N. Kim Theodore and G. M. James Doug, "Wavelet turbulence for fluid simulation," *ACM Trans. Graph.*, vol. 27, no. 3, pp. 1–6, 2008.

[11] F. Losasso, T. Shinar, A. Selle, and R. Fedkiw, "Multiple interacting liquids," *ACM Trans. Graph.*, vol. 25, no. 3, pp. 812–819, Jul. 2006.

[12] X. He, H. Wang, F. Zhang, H. Wang, G. Wang, and K. Zhou, "Robust simulation of sparsely sampled thin features in sph-based free surface flows," *ACM Trans. Graph.*, vol. 34, no. 1, Dec. 2014.

[13] H. Wang, P. J. Mucha, and G. Turk, "Water drops on surfaces," *ACM Trans. Graph.*, vol. 24, no. 3, pp. 921–929, 2005.

[14] O. Mercier, C. Beauchemin, N. Thuerey, T. Kim, and D. Nowrouzezahrai, "Surface turbulence for particle-based liquid simulations," *ACM Trans. Graph.*, vol. 34, no. 6, 2015.

[15] M. Becker and M. Teschner, "Weakly compressible sph for free surface flows," in *Acm Siggraph/eurographics Symposium on Computer Animation*, 2007.

[16] J. Bender and D. Koschier, "Divergence-free smoothed particle hydrodynamics," in *Proceedings of the 14th ACM SIGGRAPH/Eurographics Symposium on Computer Animation*. ACM, 2015, pp. 147–155.

[17] D. Gerszewski, H. Bhattacharya, and A. W. Bargteil, "A point-based method for animating elastoplastic solids." New York, NY, USA: Association for Computing Machinery, 2009, pp. 133–138.

[18] J. Onderik, M. Chládek, and R. Ďurikovič, "Sph with small scale details and improved surface reconstruction," in *Proceedings of the 27th Spring Conference on Computer Graphics*. ACM, 2011, pp. 29–36.

[19] F. de Goes, C. Wallez, J. Huang, D. Pavlov, and M. Desbrun, "Power particles: an incompressible fluid solver based on power diagrams." *ACM Trans. Graph.*, vol. 34, no. 4, Jul. 2015.

[20] X. Yan, Y.-T. Jiang, C.-F. Li, R. R. Martin, and S.-M. Hu, "Multiphase sph simulation for interactive fluids and solids," *ACM Trans. Graph.*, vol. 35, no. 4, p. 79, 2016.

[21] J. Gregson, M. Krimerman, M. B. Hullin, and W. Heidrich, "Stochastic tomography and its applications in 3d imaging of mixing fluids." *ACM Trans. Graph.*, vol. 31, no. 4, Jul. 2012.

[22] T. Lenaerts, B. Adams, and P. Dutré, "Porous flow in particle-based fluid simulations," *ACM Trans. Graph.*, vol. 27, no. 3, 2008.

[23] B. Solenthaler and R. Pajarola, "Predictive-corrective incompressible sph," *ACM Trans. Graph.*, vol. 28, no. 3, 2009.

[24] I. Markus, C. Jens, S. Barbara, H. Christopher, and T. Matthias, "Implicit incompressible sph," *IEEE Transactions on Visualization and Computer Graphics*, vol. 20, no. 3, pp. 426–435, 2014.

[25] D. Baraff and A. Witkin, "Large steps in cloth simulation," in *Proceedings of the 25th Annual Conference on Computer Graphics and Interactive Techniques*, ser. SIGGRAPH 1998. New York, NY, USA: Association for Computing Machinery, 1998, pp. 43–54.

[26] D. House and D. Breen, *Cloth Modeling and Animation*. A K Peters/CRC Press, 2000.

[27] Y.-J. Liu, D.-L. Zhang, and M.-F. Yuen, "A survey on cad methods in 3d garment design," *Computers in Industry*, vol. 61, no. 6, pp. 576–593, 2010.

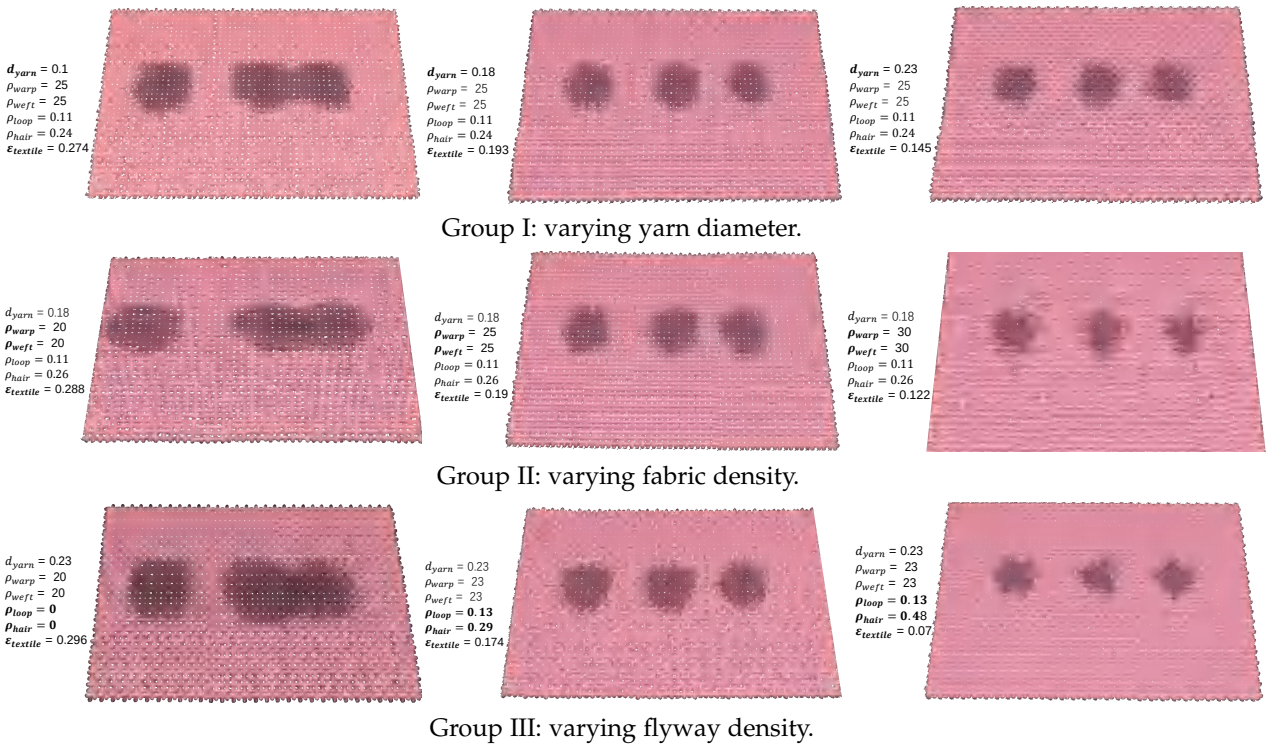

Fig. 13: Simulation of one droplet of liquid spreading on a cotton textile with different parameter settings.

(a) 3D VR application

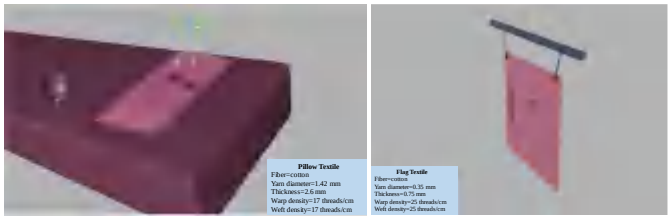

Animation scenario1 Animation scenario2

(b) Physical visualization animation

Fig. 14: Examples of physics-driven graphics application.

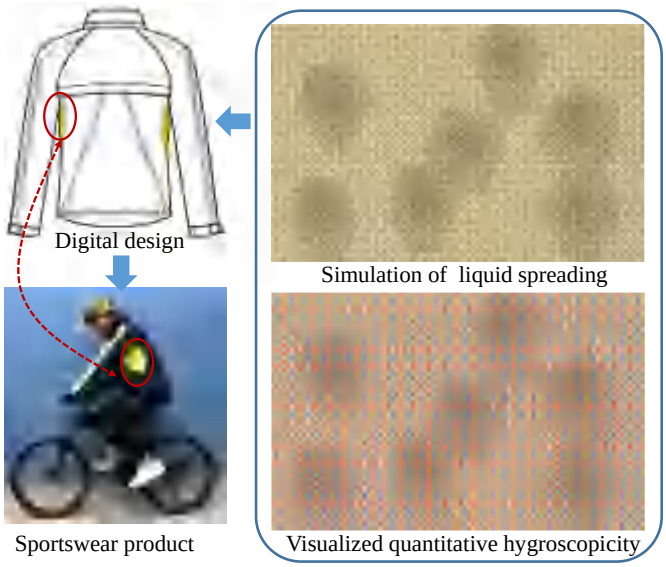

Fig. 15: An example of computer-aided design for a sportswear.

[28] S. Patkar and P. Chaudhuri, "Wetting of porous solids," *IEEE transactions on visualization and computer graphics*, vol. 19, no. 9, pp. 1592–1604, 2013.
[29] Y. Chen, N. Magnenat Thalmann, and B. Foster Allen, "Physical simulation of wet clothing for virtual humans," *The Visual Computer*, vol. 28, no. 6-8, pp. 765–774, Jun. 2012.
[30] P.-G. De Gennes, F. Brochard-Wyart, and D. Quéré, *Capillarity and wetting phenomena: drops, bubbles, pearls, waves*. Springer Science & Business Media, 2013.
[31] Y.-L. Hsieh, "Liquid transport in fabric structures," *Textile Research Journal*, vol. 65, no. 5, pp. 299–307, 1995.
[32] E. W. Washburn, "The dynamics of capillary flow," *Phys. Rev.*, vol. 17, pp. 273–283, Mar 1921.
[33] Y. Li and B. V. Holcombe, "A two-stage sorption model of the coupled diffusion of moisture and heat in wool fabrics," *Textile Research Journal*, vol. 62, no. 4, pp. 211–217, 1992.
[34] D. Lukas, E. Glazyrina, and N. Pan, "Computer simulation of liquid wetting dynamics in fiber structures using the ising model," *Journal of the Textile Institute*, vol. 88, no. 2, pp. 149–161, 2009.
[35] A. Patnaik, R. S. Rengasamy, V. K. Kothari, and A. Ghosh, "Wetting and wicking in fibrous materials," *Textile Progress*, vol. 38, no. 1,

pp. 1–105, 2006.
[36] Y. Li and Q. Zhu, "Simultaneous heat and moisture transfer with moisture sorption, condensation, and capillary liquid diffusion in porous textiles," *Textile Research Journal*, vol. 73, no. 6, pp. 515–524, 2003.
[37] A. Mao and Y. Li, "Numerical heat transfer coupled with multidimensional liquid moisture diffusion in porous textiles with a measurable-parameterized model," *Numerical Heat Transfer, Part A: Applications*, vol. 56, no. 3, pp. 246–268, 2009.
[38] N. Adabala, N. Magnenat-Thalmann, and G. Fei, "Visualization of woven cloth," in *Proceedings of the 14th Eurographics Workshop on Rendering*, ser. EGRW'03, 2003, pp. 178–185.
[39] W. Jakob, A. Arbree, J. T. Moon, K. Bala, and S. Marschner, "A radiative transfer framework for rendering materials with anisotropic structure," in *ACM SIGGRAPH 2010 Papers*, ser. SIGGRAPH '10. New York, NY, USA: Association for Computing Machinery, 2010.
[40] J. Zhang, G. Baciu, D. Zheng, C. Liang, G. Li, and J. Hu, "Idss: A novel representation for woven fabrics," *IEEE Transactions on Visualization and Computer Graphics*, vol. 19, no. 3, pp. 420–432, 2013.
[41] G. Cirio, J. Lopez-Moreno, D. Miraut, and M. A. Otaduy, "Yarn-level simulation of woven cloth," *ACM Trans. Graph.*, vol. 33, no. 6, pp. 1–11, 2014.
[42] S. Zhao, F. Luan, and K. Bala, "Fitting procedural yarn models for realistic cloth rendering," *ACM Trans. Graph.*, vol. 35, no. 4, Jul. 2016.
[43] M. Müller, D. Charypar, and M. Gross, "Particle-based fluid simulation for interactive applications," in *Proceedings of the 2003 ACM SIGGRAPH/Eurographics symposium on Computer animation*. Eurographics Association, 2003, pp. 154–159.
[44] J. P. Morris, "Simulating surface tension with smoothed particle hydrodynamics," *International journal for numerical methods in fluids*, vol. 33, no. 3, pp. 333–353, 2000.
[45] E. Kissa, "Wetting and wicking," *Textile Research Journal*, vol. 66, no. 10, pp. 660–668, 1996.
[46] A. Patnaik, R. Rengasamy, V. K. Kothari, and A. Ghosh, "Wetting and wicking in fibrous materials," *Textile Progress*, vol. 38, no. 1, pp. 1–105, 2006.
[47] I. Watt, "Kinetic study of the wool-water system: Part ii: The mechanisms of two-stage absorption," *Textile Research Journal*, vol. 30, no. 9, pp. 644–651, 1960.
[48] A. K. Haghi, *Heat & Mass Transfer in Textiles*. WSEAS Press, 2011.
[49] P. Nordon and H. David, "Coupled diffusion of moisture and heat in hygroscopic textile materials," *International Journal of Heat and Mass Transfer*, vol. 10, no. 7, pp. 853–866, 1967.
[50] B. Farnworth, "A numerical model of the combined diffusion of heat and water vapor through clothing," *Textile Research Journal*, vol. 56, no. 11, pp. 653–665, 1986.
[51] M. Ihmsen, J. Orthmann, B. Solenthaler, A. Kolb, and M. Teschner, "SPH Fluids in Computer Graphics," in *Eurographics 2014 - State of the Art Reports*, S. Lefebvre and M. Spagnuolo, Eds. The Eurographics Association, 2014.
[52] A. T. M. 195-2011, "Liquid moisture management properties of textile fabrics," AATCC, Tech. Rep., 2009.
[53] B. guo Yao, Y. Li, J. yan Hu, Y. lin Kwok, and K. wing Yeung, "An improved test method for characterizing the dynamic liquid moisture transfer in porous polymeric materials," *Polymer Testing*, vol. 25, no. 5, pp. 677 – 689, 2006.
[54] J. J. Lee and D. S. Ji, "Evaluation of liquid moisture management properties on hemp woven fabrics treated with liquid ammonia," *Textile Research Journal*, vol. 87, no. 14, pp. 1752–1764, 2017.
[55] F. Nielsen and R. Nock, "A fast deterministic smallest enclosing disk approximation algorithm," *Information Processing Letters*, vol. 93, no. 6, pp. 263–268, 2005.

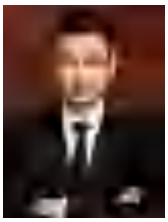

Aihua Mao is a professor with the School of Computer Science and Engineering, South China University of Technology (SCUT), China, He received the PhD degree from the Hong Kong Polytechnic University in 2009, the M.Sc degree from Sun Yat-Sen University in 2005 and the B.Eng degree from Hunan University in 2002. His research interests include 3D vision and computer graphics.

Wenbo Dong is a M.Sc student with the School of Computer Science and Engineering, South China University of Technology (SCUT), China. He received his B.Eng. degree from Southwest Jiaotong University, China, in 2017. His research interests include computer-aided design and computer graphics.

Chaoqiang Xie is a M.Sc student with the School of Software Engineering, South China University of Technology (SCUT), China. He received his B.Eng. degree from Anhui Agricultural University, China, in 2019. His research interests include software engineering and computer graphics.

Huamin Wang received the BEng degree from Zhejiang University, in 2002, the MS degree from Stanford University, in 2004, and the PhD degree in computer science from Gerogia Institute of Technology, in 2009. He is currently an associate professor in the Department of Computer Science and Engineering, Ohio State University. Before joining Ohio State University, he was a postdoctoral researcher in the Department of Electrical Engineering and Computer Sciences, University of California, Berkeley.

Yong-Jin Liu is a professor with the Department of Computer Science and Technology, Tsinghua University, China. He received the BEng degree from Tianjin University, China, in 1998, and the PhD degree from the Hong Kong University of Science and Technology, Hong Kong, China, in 2004. His research interests include computer graphics and computer-aided design.

Guiqing Li received the BS degree in mathematics from the University of Science and Technology of China, MS degree from Naikai University, and PHD degree of computer application from Chinese Academy of Science. He is a professor of computer science and engineering at South China University of Technology. His main research interests include digital geometry processing and reverse engineering.

Ying He is an associate professor in the School of Computer Engineering, Nanyang Technological University, Singapore. He received his Bachelor (1997) and Master (2000) degrees in Electrical Engineering from Tsinghua University, and PhD (2006) in Computer Science from Stony Brook University. He is interested in the problems that require geometric computing and analysis. He is now an Associate Editor of IEEE Trans. Visualization and Computer Graphics.

Yarn-Level Simulation of Hygroscopicity of Woven Textiles (Appendix)

Aihua Mao, Wenbo Dong, Chaoqiang Xie, Huamin Wang, Yong-Jin Liu,Guiqing Li, Ying He

In this appendix, we present the equation solvers and a nomenclature for the physics models Eqs.(3)-(11) presented in the paper.

A1 Equation solvers

In Section 6.1 of this paper, we present a group of physic models for describing the liquid diffusion across a textile. In this section we give out equation solvers for these models corresponding to the illustration in Fig.5.

First, Eq.(3) can be deduced to calculate the surface tension fiber-liquid interface(γ_{sl}):

$$\gamma_{sl} = \gamma_{lv}\cos\theta - \gamma_{sv} \tag{A1}$$

where the value of γ_{lv} of water can be found in [1], such as 0.0728 N/m at temperature 20°C, the value of γ_{sv} of cotton fibers can be found in [2], θ is the contact angle measuring the wettability of a textile. Then the surface tension force F_i^o in Eq.(11) can be obtained by $F_i^o = \gamma_{sl} * d_p$, where d_p is the diameter of the liquid particle. In physics, F_i^o acts along the tangent at the point of contact.

Then, Eq.(4) can calculate the net pressure $\Delta P = P - \rho_l g h$, where $P = \frac{2\gamma_{lv}\cos\theta}{R_c}$ and h can be be calculated by $h = \frac{2\cos\theta F_i^o}{R_c \rho_l g}$ [3]. Thus, the capillary force F_i^c on the particle area in Eq.(11) can be calculated by $F_i^c = \Delta P * 2\pi(d_p/2)^2$.

Since Eq.(6)-(9) are partial differential equation, they are solved by the finite-volume method (FVM) (details can be found in [4]). To solve Eq.(6) for moisture sorption/desorption rate of the fiber, it can be expressed in the integral form:

$$\int_\Omega \left(r\frac{\partial C_f}{\partial t}\right) dr = \int_\Omega \left(\frac{\partial}{\partial r}\left(r D_f \frac{\partial C_f}{\partial r}\right)\right) dr \tag{A2}$$

and then it is discretized as:

$$\begin{aligned} \left(\mu\eta r_{i-\frac{1}{2}} D^n_{f,i-\frac{1}{2}}\right) C^{n+1}_{f,i-1} - \\ \left(\mu\eta r_{i+\frac{1}{2}} D^n_{f,i+\frac{1}{2}} + \mu\eta r_{i-\frac{1}{2}} D^n_{f,i-\frac{1}{2}} + 1\right) C^{n+1}_{f,i} \quad + \\ \left(\mu\eta r_{i+\frac{1}{2}} D^n_{f,i+\frac{1}{2}}\right) C^{n+1}_{f,i+1} = -C^n_{f,i} \end{aligned} \tag{A3}$$

where $\mu = \frac{\Delta t}{\Delta r^2}$ and $\eta = \frac{2}{r_{i-1}+r_{i+1}}$. Γ_f in Eqs.(7)-(9) refers to the sum of moisture sorption/desorption rate of all composited fibers in the yarn, and thus can be calculated by $\Gamma_f = \sum_{ti=1}^{n} (C_f)_{ti}$.

Eqs.(7)-(9) are solved by dividing the textile into a number of grids consisting of control cells with equal interval size, and the equation can be discretized on a control volume Ω.

With FVM, Eq.(7) is firstly re-written as the integral form:

$$\int_\Omega \left[A\frac{\partial C_a}{\partial t} - E + \Gamma_{lg}\right] dx = \int_\Omega \left[\frac{\partial}{\partial x}\left(D\frac{\partial C_a}{\partial x}\right)\right] dx \tag{A4}$$

where $A = \varepsilon_a$, $E = \omega_a \varepsilon_f \frac{\partial C_f}{\partial t}$, $\Gamma_{lg} = h_{lg} S_v \left(C_a^*(T) - C_a\right)$, $D = D_a \frac{\varepsilon_a}{\tau_a}$, $\mu = \frac{\Delta t}{\Delta t^2}$.

Then, the discretized equation of Eq.(7) for numerical solution can be obtained as:

$$\begin{aligned} \left(\mu_{i-1} D^n_{i-\frac{1}{2}}\right) C^{n+1}_{a,i-1} + \left(\mu_{i+1} D^n_{i+\frac{1}{2}}\right) C^{n+1}_{a,i+1} - \\ \left(A^n_i - \mu_{i+1} D^n_{i+\frac{1}{2}} + \mu_{i-1} D^n_{i-\frac{1}{2}}\right) C^{n+1}_{a,i} = \\ A^n_i C^n_{a,i} - E^n_i \Delta t + (\Gamma_{lg})^n_i \Delta t \end{aligned} \tag{A5}$$

Similarly, the discretized equation of Eq.(8) for numerical solution can be obtained as:

$$\begin{aligned} \left(\mu_{i-1} L^n_{i-\frac{1}{2}}\right) \varepsilon^{n+1}_{l,i-1} + \left(\mu_{i+1} L^n_{i+\frac{1}{2}}\right) \varepsilon^{n+1}_{l,i+1} - \\ \left(A^n_i + \mu_{i-1} L^n_{i-\frac{1}{2}} + \mu_{i+1} L^n_{i+\frac{1}{2}}\right) \varepsilon^{n+1}_{l,i} = \\ A^n_i \varepsilon^n_{l,i} - E^n_i \Delta t - (\Gamma_{lg})^n_i \Delta t \end{aligned} \tag{A6}$$

- *A.H. Mao, W.B. Dong and G.Q. Li are with School of Computer Science and Engineering, South China University of Technology, Guangzhou, China. E-mails: {ahmao|875158248|ligq}@scut.edu.cn.*
- *C.Q Xie is with School of Software Engineering, South China University of Technology, Guangzhou, China. E-mails: 201921043082@mail.scut.edu.cn.*
- *H.M. Wang (corresponding author) is with Department of Computer Science and Engineering, The Ohio State University, Columbus, OH 43210-1277, USA. E-mail: whmin@cse.ohio-state.edu.*
- *Y.-J. Liu is with BNRist, MOE-Key Laboratory of Pervasive Computing, Department of Computer Science and Technology, Tsinghua University, Beijing, China. E-mail: liuyongjin@tsinghua.edu.cn.*
- *Y. He is with School of Computer Science and Engineering, Nanyang Technological University, Singapore. E-mail: yhe@ntu.edu.sg.*

where $A = \rho_l$, $E = \omega_l \varepsilon_f \frac{\partial C_f}{\partial t}$, $L = \frac{\rho_l}{\tau_l} D_l$.

And the discretized equation of Eq.(9) for numerical solution can be obtained as:

$$\begin{aligned} &\left(\mu K^n_{i-\frac{1}{2}}\right) T^{n+1}_{i-1} + \left(\mu K^n_{i+\frac{1}{2}}\right) T^{n+1}_{i+1} - \\ &\left(A^n_i + \mu K^n_{i-\frac{1}{2}} + \mu K^n_{i+\frac{1}{2}}\right) T^{n+1}_i = -A^n_i T^n_i + Q^n_i \Delta t \end{aligned} \tag{A7}$$

where $A = c_v$, $Q = \kappa \varepsilon_f \Gamma_f - \lambda_{lg} \Gamma_{lg}$.

For Eq.(11), the term F^p_i is calculated by the pressure fore between liquid particles (F^{par}_i) and diffusion gradient (F^{dif}_i), namely:

$$F^p_i = F^{par}_i + F^{dif}_i \tag{A8}$$

where, F^{par}_i can be calculated being similar to Eq.(2), namely, $F^{par}_i = \sum_j V_j \left(\frac{|\nabla p_i|^2 + |\nabla p_j|^2}{2}\right) \nabla_i W^h_{ij}$, p is the pressure of a particle surrounding. F^{dif}_i can be calculated by the C_a solution from Eq.(7), namely, $F^{dif}_i = \sum_j (C_{a,i} - C_{a,j})(t + 273.16)/0.002166$, t is air temperature.

F^v_i in Eq.(11) is also calculated being similar to Eq.(2), namely, $F^v_i = \sum_j \mu V_j \left(v_j - v_i\right) \nabla_i W^h_{ij}$, μ is viscosity coefficient of liquid, v is the velocity of particle.

The calculation of F^c_i in Eq.(11) is obtained by $F^c_i = \Delta P * 2\pi (d_p/2)^2$ as discussed in above, and F^o_i could be the solution of Eq.(3) on liquid surface or $F^o_i = \gamma_{sl} * d_p$ on the fiber-liquid interface, or even frictional force on the contact surface between fiber and liquid.

A2 NOMENCLATURE

In this section, all the variables and parameters used in Eqs.(3)-(9) for the physics models are listed in table A1. The default values or calculation methods of the parameters are also demonstrated. It is noted that the values of the parameters could be different for different cases.

REFERENCES

[1] J. G. Speight, "2 - the properties of water," in *Natural Water Remediation*, J. G. Speight, Ed. Butterworth-Heinemann, 2020, pp. 53–89.
[2] "A study of the surface properties of cotton fibers by inverse gas chromatography," *Journal of Colloid and Interface Science*, vol. 314, no. 2, pp. 373–380, 2007.
[3] G. of Tamil Nadu, *11th Physics : Properties of Matter : Surface Tension by capillary rise method*. Tamil NaduTextbook and Educational Services Corporation, 2018.
[4] M. Aihua and L. Yi, "Numerical heat transfer coupled with multidimensional liquid moisture diffusion in porous textiles with a measurable-parameterized model," *Numerical Heat Transfer, Part A: Applications*, vol. 56, no. 3, pp. 246–268, 2009.

TABLE A1
Variables and parameters used for physics models

Symbols	Definition	Value and unit
C^*	saturated water vapor concentration at a local temperature	k/m^3
C_a	water vapor concentration in the air filling the inter-fiber void space	k/m^3
C_f	water vapor concentration in the fibers of the material	k/m^3
c_v	volumetric heat capacity of the textile	$5.64 \times 10^3 \times \frac{(0.32+w_c)}{(1.0+w_c)} k/m^3$
D_a	diffusion coefficient of water vapor in the air of the textile	$2.2 \times 10^{-5} m^2/s$
D_f	diffusion coefficient of water vapor in the fibers of the textile	$(50.6w_c - 1100w_c^2) \times 10^{-13} m^2/s$
D_l	diffusion coefficient of liquid water in the textile	$\frac{3\gamma_{sl}\cos\theta \sin^2\beta R_c \varepsilon_l}{20\eta\varepsilon} m^2/s$
Γ_f	water vapor sorption/desorption rate by the fiber	$\%$
Γ_{lg}	evaporation/condensation rate of the moisture	$h_{\mathrm{lg}} S_v \left(C^*(T) - C_a\right) \%$
h	wicking height of a capillary tube	m
h_{eq}	equilibrium wicking height of a capillary tube	$\frac{2\gamma_{lv}\cos\theta}{R_c \rho_l g} m$
h_{lg}	mass transfer coefficient for evaporation and condensation	$0.17 m/s$
K	effective thermal conductivity of the textile	$(44.1 + 63.0w_c) \times 10^{-3} W/m.K$
P	pressure of a capillary tube	$\frac{2\gamma_{lv}\cos\theta}{R_c} Pa$
R_c	radius of a capillary tube	$0.2 \times 10^{-3} m$
r	fiber radius in radial coordinate (cotton)	m
S_v	surface volume ratio of the fiber	$\frac{2}{r}/m$
T	temperature of the fabric	K
w_c	absorbed water content in the fiber	$\%$
ε_a	volume fraction of water vapor of the textile	$(1 - \varepsilon_f - \varepsilon_l) \%$
ε_l	volume fraction of liquid of the textile	$\%$
ε_f	volume fraction of fibers of the textile	$\frac{\rho_{\mathrm{fabric}}}{\rho_{\mathrm{fiber}}} \%$
ε	porosity of the fabric	$(1 - \varepsilon_f) \%$
γ_{sv}	surface tension at the textile-vapor (cotton at 30°C)	$42 N/m$
γ_{sl}	surface tension at the textile-liquid	N/m
γ_{lv}	surface tension at the liquid-vapor (water)	$0.0728 N/m$
θ	contact angle between liquid-vapor and solid-liquid interfaces	$\circ$
β	intersection angle between the barycenter of yarn segment and gravity	$20°$
ρ_l	density of liquid (water)	$1 \times 10^3 kg/m^3$
ρ_{fiber}	density of fiber (cotton)	$1.52 \times 10^3 kg/m^3$
ρ_{fabric}	density of fabric	kg/m^3
η	dynamic viscosity of liquid water (cotton)	$1.0 \times 10^{-3} kg/m.s$
λ_v	latent heat of sorption of vapor	$2522 kJ/kg$
λ_l	latent heat of sorption of liquid	$1.6025 e^{-8.72} kJ/kg$
ω_a	proportion of the sorption of water vapor at the fiber surface	$\frac{\varepsilon_a}{\varepsilon} \cdot \varepsilon_f$
ω_l	proportion of the sorption of liquid at the fiber surface	$(1 - \omega_a)$
τ_a/τ_l	effective tortuosity of the textile for water vapor/liquid diffusion	1.2